Magnetohydrodynamic (MHD) and Radiation Effect on the Casson Nanofluid Flow over Linear Stretching Sheet.

Hazoor Bux Lanjwani[1, a)] M Imran Anwar[2, b)] and M Saleem Chandio[1, c)] Sumera Dero[1, d)] and Liaquat Ali Lund[3, d)]

[1]*University of Sindh, Jamshoro, Pakistan.*
[2]*Engineering University Sargodha Punjab, Pakistan.*
[3]*KCAET Khairpur, Sindh Agriculture University, Tandojam, Pakistan.*

a) **hazoor.bux@scholars.usindh.edu.pk**
b) **jeotarar@yahoo.com**
c) **mschandio@hotmail.com**
d) **sumera.dero@usindh.edu.pk**
e) **balochliaqatali@gmail.com**

a) Corresponding author: hazoor.bux@scholars.usindh.edu.pk

Abstract

In this paper, Magnetohydrodynamic (MHD) flow of the Casson based nanofluid has been studied in presence of thermal radiation effect towards a linear stretching sheet. The governing equations are reduced in the form of the ordinary differential equations by using similarity transformations. The reduced equations are solved by shooting technique with Runge Kutta method MAPLE software implementation. In order to validate the accuracy of shooting method, numerically obtained results of the skin friction and the Nusselt number are compared with three-stage-Labattoo-three-A-formula in bvp4c ODE solver and found in the excellent agreements. The effect of Casson, magnetic, thermal radiation, the thermophoresis and the Brownian motion parameters on the velocity, temperature and the concentration profiles have been taken in the account. The results reveal that thickness of momentum boundary layer declines as the values of magnetic, Casson parameters are increased. Furthermore, temperature of fluid increases when thermophoresis and the Brownian motion of particles are enhanced. In last, the values of skin friction coefficient, Nusselt as well as Sherwood numbers are gotten for the different values of applied parameters shown in the tables.

Keyword: Nanofluid, Thermal Radiation, Stretching surface, Revised Model.

Introduction

Many researchers are attracted towards the investigation of the boundary layer, heat and mass transfer flows through stretching surfaces/sheets due to possessing vast applications in various engineering fields and industries. Some of the important applications are in aerodynamics, hot rolling, extrusion of the plastic sheets, artificial fibers, metal spinning, lubricant, paper production, drawing of the plastic films, wire drawing, glass fiber production etc. At first, the pioneering work on the stretching surface was performed by Crane [1], he worked on steady boundary flow due to linear stretching surface whereas Gupta et al., [2] studied Heat and mass transfer past over stretching plate surface. After that, the study over a different type of stretching surfaces was performed by many other researchers. The Grubka and Bobba [3] investigated the flow on the stretching surface. Furthermore, the studies concerned with stretching surfaces were performed by [4–6].

Nowadays, it is noted that energy efficiency is a main important topic in view of the thermal conductivity enhancement, mostly researchers considered different base fluids along with nano-sized various particles for this purpose. the researchers considered the involvement of nano-sized particles in the commonly used base fluid. The nanofluids might be utilized as a working fluid instead of simple common base fluids due to possessing high thermal conductivity. Choi [7] was the first investigator who prepared such fluid by suspending nano-size particles in the simple base fluid that are later named as nanofluid. It is proved that nanofluid possess higher thermal conductivity as compared to base fluids. Nanofluids can be used in various energetic systems like as natural convection in enclosures, radiators, cooling of the nuclear systems, etc. in the future modern science and technology. Lee et al., [8] stated that the nanofluids possess outstanding heat transfer characteristics when they are compared to the common base fluids. Additionally, many other researchers [9–14] have shown that the nanofluids possess greater thermo-physical and heat transfer characteristics as compare to commonly base fluids. Buongiorno [15] proposed the nanofluid model to explore the properties of the enhancement of the heat transfer in the nanofluids. Recently, many investigators have used Buongiorno's model successfully with necessary modification according to their study. Khan and Pop [16] analyzed the two-dimensional steady boundary layer nanofluid flow through the stretching sheet initially. The effects of the thermophoresis and the Brownian motion on free convection boundary layer flow on a porous vertical plate was examined by Nield and Kuznetsov [17]. Rana et al., [18] studied the Brownian

motion and the thermophoresis effect on mixed convection boundary layer steady nanofluid flow of on inclined porous plate numerically. Makinde and Aziz [19] examined the effect of the Brownian motion, thermophoresis and the convective boundary conditions on two-dimensional steady boundary layer nanofluid flow past on stretching sheet. Afify and Bazid [20] analyzed the effect of the variable nanofluid properties along with the thermophoresis and the Brownian motion at a free convective boundary layer flow through the vertical plate. Recently, Makinde et al., [21] considered the effect of the variable viscosity, magnetic field and the thermal radiation on the convective heat transfer of the nanofluid through stretching sheet. Mustafa et al., [22] analyzed the boundary layer nanofluid flow through the exponential stretching surface by considering convective boundary conditions.

The non-Newtonian based nanofluids can widely be considered in different technological and industrial applications, like as, the dissolved polymers, paints, biological solutions, glues, and asphalt etc. Casson fluid model is classified as a sub-class of the non-Newtonian fluid. It is a rheological model for different fluids like chocolate and blood. Casson fluid model shows yield stress. These fluid acts like a solid when the yield stress is greater than shear stress. It starts deforming when the yield stress becomes lesser than shear stress. These types of fluids hold many applications in metallurgy, food processing, bioengineering operations, and drilling operations. The Casson in 1959 discovered this model which now known as a Casson fluid model especially to find the flow characteristics of the pigment-oil suspension [23]. Later on, many researchers [24–25] considered the boundary layer Casson fluid flow of simply and the Casson nanofluid flow at various geometrical regimes. Mustafa et al. [26] analytically worked on unsteady boundary layer Casson fluid flow through the moving flat plate, to get an analytical solution he applied the homotopy analysis method. Nadeem et al. [27] found analytical solutions of convective boundary conditions for the steady stagnation-point flow of a Casson nanofluid. Makanda et al. [28] studied MHD Casson fluid flow on the stretching sheet saturated in the porous medium along with the effect of the chemical reaction numerically.

The previously published work indicates that there has been given a little attention given to the non-Newtonian based nanofluids. The main purpose of this work is to extend the work of the Khan and Pop (2010) under consideration of thermal radiation effect on Casson type nanofluid. The main purpose of the investigation is to examine the steady MHD boundary layer flow of Casson

based nanofluid, using of Buongiorno model (2006), over linear stretching sheet along with thermal radiation. The governing partial differential equations along with subjected boundary conditions are reduced in the form of the ordinary differential equations by applying similarity transformations. Moreover, reduced ordinary differential equations are solved by applying shooting technique by the help of MAPLE software. The obtained numerical results are plotted and discussed to clarify the physical aspects of the problem. Skin-friction coefficient, the Nusselt number, and the Sherwood number have been discussed at the different values of applied physical parameters that are included in the present study.

Mathematical Formulation

There has been considered steady two-dimensional incompressible MHD flow of a Casson based nanofluid on a linearly stretching sheet along with radiation effect. Cartesian coordinates x is taken along sheet with u as a velocity component and y normal to the sheet with v velocity component. The flow is produced because of the stretching sheet. The sheet is stretched with a linear velocity $u_w(x) = ax$ where a is positive constant related to the stretching sheet, keeping the origin fixed. The momentum, temperature and the concentration equations following above-mentioned conditions are written as.

$$\frac{\partial u}{\partial x} + \frac{\partial v}{\partial y} = 0 \quad (1)$$

$$u\,\frac{\partial u}{\partial x} + v\,\frac{\partial u}{\partial y} = \vartheta\left(1 + \frac{1}{\beta}\right)\frac{\partial^2 u}{\partial y^2} - \frac{\sigma B^2 u}{\rho_f} \qquad (2)$$

$$u\,\frac{\partial T}{\partial x} + v\,\frac{\partial T}{\partial y} = \alpha\,\frac{\partial^2 T}{\partial y^2} + \tau\left[D_B\,\frac{\partial C}{\partial y}\,\frac{\partial T}{\partial y} + \frac{D_T}{T_\infty}\left(\frac{\partial T}{\partial y}\right)^2\right] - \frac{1}{(\rho c)_f}\frac{\partial q_r}{\partial y} \quad (3)$$

$$u\,\frac{\partial C}{\partial x} + v\,\frac{\partial C}{\partial y} = D_B\,\frac{\partial^2 C}{\partial y^2} + \frac{D_T}{T_\infty}\,\frac{\partial^2 T}{\partial y^2} \qquad (4)$$

The expression for Roseland term is given as (please provide one reference),

$$q_r = -\frac{4\sigma^*}{3K^*}\frac{\partial^2 T}{\partial y^2}, \quad (5)$$

where σ^* classifies the expression for Stefan-Boltzmann activated in the thermal layer in addition to K^*gives the mean absorption coefficient. Also, the streaming for the temperature diversity is classified as the streaming to be free T_∞ and at local T that is considered to be very small, the series expansions in T^4 by means of Taylor expressions with T_∞ by and discarding the higher indexed results for

$$T^4 = 4\left(T_\infty{}^3\right)T - 3(T_\infty{}^4) \quad (6)$$

After substituting equation (5) and (6), equation (3) reduces to;

$$u\,\frac{\partial T}{\partial x} + v\,\frac{\partial T}{\partial y} = \left(\alpha + \frac{16\sigma^*}{3K^*(\rho c)_f}\right)\frac{\partial^2 T}{\partial y^2} + \tau\left[D_B\,\frac{\partial C}{\partial y}\,\frac{\partial T}{\partial y} + \frac{D_T}{T_\infty}\left(\frac{\partial T}{\partial y}\right)^2\right] \quad (7)$$

The subject to boundary conditions

$$v = 0;\quad u = u_w(x) = ax;\quad T = T_w(x);\quad C = C_w(x)\quad at\quad y = 0$$

$$u \to 0;\quad T \to T_\infty;\quad C \to C_\infty \text{ as } y \to \infty \quad (8)$$

here, u and v are velocity components along with respective directions *x*-axis and *y*-axis. The ϑ is the kinematic viscosity, $\beta = k_c\sqrt{2\pi_C}\,/\tau_0$ indicates Casson fluid parameter, σ electrical conductivity, the thermal diffusivity is denoted by α . Furthermore, *T* denotes the temperature at boundary layer, $T_w(x)$ stands for the variable temperature of the surface and T_∞ free stream temperature, $\tau = {(\rho c)_p}\big/{(\rho c)_f}$ indicates the ratio of the heat capacity of nano-sized particle to the heat capacity of base fluid. The D_T and D_B are the coefficients of the thermophoresis and Brownian diffusions respectively. *C* denotes the concentration at the boundary layer, $C_w(x)$ stands for the variable of the concentration sheet and C_∞ free stream concentration. The velocity components in term of stream functions are written as.

$$u = \frac{\partial \psi}{\partial y} \quad \text{and} \quad v = -\frac{\partial \psi}{\partial x}$$

where, $\psi = (a\vartheta)^{\frac{1}{2}} x f(\eta)$ in $f(\eta)$ which indicate dimensionless stream function $\eta = \left(\frac{a}{\nu}\right)^{\frac{1}{2}} y$ is similarity variable. According to given transformation the velocity components u and v are written as

$$u = axf'(\eta) \text{ and } v = -(a\vartheta)^{\frac{1}{2}} f(\eta) \tag{9}$$

The transformations for the temperature and concentration is given by

$$\theta(\eta) = \frac{T - T_\infty}{T_w - T_\infty} \text{ and } \emptyset(\eta) = \frac{C - C_\infty}{C_w - C_\infty} \tag{10}$$

Where, $\theta(\eta)$ indicate dimensionless temperature and $\emptyset(\eta)$ stands for dimensionless concentration. By apply the relation given in (9) and (10) in the equations (2)-(7) and (4) there has been obtained following reduced two-point boundary value problem.

$$\left(1 + \frac{1}{\beta}\right) f'''(\eta) + f(\eta) f''(\eta) - f'^2(\eta) - M f'(\eta) = 0 \tag{11}$$

$$\frac{1}{Pr}\left(1 + \frac{4R}{3}\right)\theta''(\eta) + f(\eta)\theta'(\eta) + Nb\phi'(\eta)\theta'(\eta) + Nt\theta'^2(\eta) = 0 \tag{12}$$

$$\phi''(\eta) + Lef(\eta)\phi'(\eta) + \frac{Nt}{Nb}\theta''(\eta) = 0 \tag{13}$$

Subject to boundary conditions

$$\begin{cases} f(0) = 0, f'(0) = 1, \theta(0) = 1, \phi(0) = 1 \\ f'(\eta) \to 0, \theta(\eta) \to 0, \phi(\eta) \to 0 \text{ as } \eta \to \infty \end{cases} \tag{14}$$

Where R is radiation parameter, $Pr = \frac{\nu}{\alpha}$ Prandtl number, $Nb = \frac{D_B(\rho C)_p(C_w - C_\infty)}{\nu(\rho C)_f}$ Brownian motion parameter, $Nt = \frac{D_T(\rho C)_p(T_w - T_\infty)}{\nu(\rho C)_f T_\infty}$ thermophoresis parameter and $Le = \frac{\vartheta}{D_B}$ Lewish number. The other physical quantities like as skin-friction coefficient, the local Nusselt and the Sherwood numbers are computed by the following equations.

$$C_f = \frac{\left[\vartheta\left(1+\frac{1}{\beta}\right)\frac{\partial u}{\partial y}\right]_{y=0}}{\rho u_w^2},\ N_u = \frac{-x\left[\left(\frac{16\sigma^* T_\infty^3}{3K^*}+k\right)\frac{\partial T}{\partial y}\right]_{y=0}}{(T_w - T_\infty)}, S_h = \frac{-x\left(\frac{\partial C}{\partial y}\right)_{y=0}}{(C_w - C_\infty)} \quad (15)$$

Using Eq. (7) in (13), we get

$$C_f (Re_x)^{\frac{1}{2}} = \left(1+\frac{1}{\beta}\right) f''(0);\ N_u (Re_x)^{-\frac{1}{2}} = -\left(1+\frac{4}{3}Rd\right)\theta'(0); S_h (Re_x)^{-\frac{1}{2}} = -\emptyset'(0) \quad (16)$$

where $Re_x = ax^2/\vartheta$ is the Reynolds number.

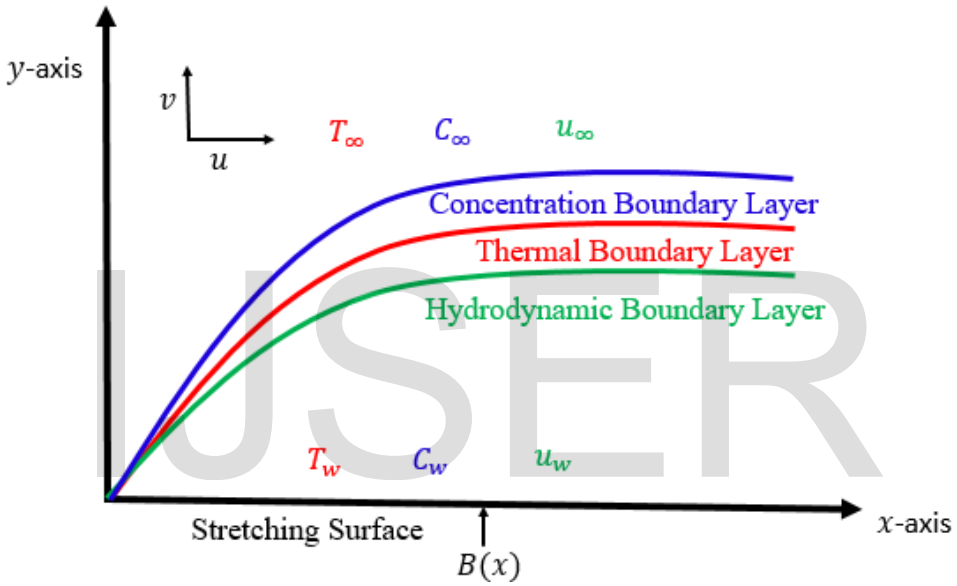

Fig 1. Physical model of Casson nanofluid.

Result and Discussion

The non-linear steady boundary layer, heat and the mass transfer of laminar incompressible Casson nanofluid flow past over a linearly stretching sheet has been considered. In order to examine the physical significance of the problem, the numerically obtained values concerned to the velocity profile $f'(\eta)$, temperature profile $\theta(\eta)$ and the concentration profile $\phi(\eta)$ are computed for pertinent parameters such as, Casson parameter β, Magnetic parameter M, the Prandtl number Pr, the Brownian motion parameter Nb, the thermophoresis parameter Nt, radiation parameter R and the Lewis number Le respectively. For the validation, the numerically obtained results are compared for skin friction values to the already reported by Ferdows, *et al.*, [29] and Khan and

Pop [11] in Table 1. The results show good agreement to the newly obtained results given thereby that develops confidence of the accuracy related to the present method. Table 2. shows the values of Skin friction co-efficient and heat and concentration transfer rate.

Table 1. Comparison of our results with previously published results when $\beta \to \infty, M = 0, and\ R = 0.$

Nb=Nt	[29]	[16]	Present results
0.1	0.9524	0.9524	0.9525
0.2	0.3653	0.3654	0.3653
0.3	0.1351	0.1355	0.1356
0.4	0.0490	0.0495	0.0497
0.5	0.0178	0.0179	0.0179

Table 2: Results of skin friction, heat transfer rate and Sherwood number for different values of applied parameters.

β	M	Pr	Nt	Le	Nb	R	$f''(0)$	$-\theta'(\eta)$	$-\phi'(\eta)$
Infi							-1.0000625	0.49544974	0.2618206
0.5							-0.5785731	0.56967455	0.3574765
1	0						-0.70759669	0.54667844	0.3259349
	0.5						-0.86606416	0.51871496	0.2896679
	1	1					-1.00000419	0.49549108	0.2619126
		3					-1.00000419	0.85112745	-0.0098374
		7.5	0.2				-1.00000419	1.152318325	-0.2497082
			0.3				-1.00000419	1.024225832	-0.4904840
			0.5	1			-1.00000419	0.81038916	-0.7268871
				2			-1.00000419	0.54656577	-0.4157432
				3	0.2		-1.00000419	0.43245605	1.0189915
					0.3		-1.00000419	0.30073026	1.22866042
					0.5	0	-1.00000419	0.13436465	1.31006171
						0.5	-1.00000419	0.24044606	1.20981252
						1	-1.00000419	0.29857379	1.14797155

Fig. 2 shows that enhancement in Casson parameter β increases fluid viscosity due to applied stress that ultimately decelerates the flow of nanofluid along the x-direction. Therefore, velocity and boundary layer thickness are decreased. The same trend of the result is observed in Fig.3 when the value of the magnetic parameter *M* is increased. Actually, as the effect of magnetic parameter *M* rises, the Lorentz forces become stronger along the direction perpendicular to x-axis that offers more resistance in the flow of the nanofluid as a result velocity of nanofluid reduces. It is noted that velocity of the nanofluid decay at the short distances from sheet in both cases, either β or *M* is increased.

The Figs. 4 and 5 indicate that the increment in Casson fluid parameter β, temperature, and the concentration distribution profiles are increased. Physically this happened due to that the greater values of β indicate stronger molecular motion as well as interactions that ultimately increases the fluid temperature and concentration rate. In result, the thickness of the thermal and the concentration boundary layers are increased. Where the same type of effect is observed in Figs. 6 and 7, when Magnetic parameter *M* is increased due to rising Lorentz forces, both the profiles temperature and concentration are increased respectively, and thermal and concentration boundary becomes thicker.

In Fig. 8, the temperature distribution profile for the different values of Prandtl number *Pr* are calculated. As by definition *Pr* is inverse proportional to thermal diffusivity, the increasing value of the *Pr* indicates a decay in the thermal diffusivity that ultimately reduces the temperature, therefore, the thermal boundary layer becomes thinner.

Fig. 9 indicates that the temperature of the nanofluid arises when Brownian motion parameter *Nb* is enhanced. Whereas, a reverse trend is examined for a concentration profile that is plotted in Fig. 10. Consequently, the thermal boundary layer thickness increases and converse to it the thickness of the concentration boundary layer decreases. This is because of the fact that Brownian motion takes place in the zig-zag path, so the kinetic energy of particles increases that consequently shows an increase in the collision of particles.

Effect of thermophoresis parameter over temperature distribution profile $\theta(\eta)$ can be seen in Fig.11. Due to thermophoretic influence, the nano-sized particles are moved away from hotter stretching sheet to the colder fluid at ambient due to the effect of the temperature gradient.

Therefore, the temperature profile $\theta(\eta)$ is the increasing function of the thermophoresis parameter *Nt*. The strong thermophoretic effect invades a larger extent of the fluid with suspended nano-sized particles, so the thermal boundary layer thickness is enhanced. The result of Fig. 12. indicates that the concentration of nanoparticle is directly proportional in thermophoresis parameter *Nt*. That is because of the diffusion penetrates deeply in the fluid when *Nt* is increased that causes the increasing of the thickness in both thermal and the concentration boundary layers.

Fig. 13 is drawn to check the influence of radiation parameter *R* at temperature distribution profile $\theta(\eta)$. It is seen that the temperature $\theta(\eta)$ increases because of the increase in radiation parameter *R*. Actually, it is because of the reason that at the larger value of *R*, the mean absorption coefficient K^* is decreased that develops divergence of radiative heat flux. The radiation parameter *R* always releases heat energy in the flow region. Therefore, the rate of the radiative heat transfer rises to nanofluid and in a result, the nanofluid temperature is increased.

The effect of the Lewis number *Le* at nanoparticles concentration profiles $\phi(\eta)$ at different values of *Le* is drawn in the Fig.14. It is examined that as the Lewis number *Le* increases, the concentration boundary layer thickness decreases. Actually, the greater value of Lewis number increases the concentration rate of the nanoparticles in the nanofluid, so in the result, the concentration profiles are decreased. The combined effect of radiation parameter *R* and Lewis number *Le* on concentration profile is plotted in Figs. 15. From this plot, it is clear that the rate of concentration decreases as the rate of the radiation parameter *R* and Lewis number *Le* increase. Therefore, the concentration boundary layer becomes thinner.

Fig. 16-17 show the influence of thermophoresis parameter on heat and concentration transfer rate. As thermophoresis increases, rate of heat decreases. On the other hand, Concentration rate enhances when thermophoresis increases. The effect of Brownian motion on heat and concentration transfer are shown in Fig. 18-19. It can be seen that heat transfer rate decreases when Brownian motion increases while opposite trend has been noticed for concentration rate.

Conclusion

The boundary layer Casson nanofluid flow over linear stretching surface is examined. The numerical computations are performed by using the shooting approach along with fourth order Runge-Kutta method. The main findings of the present study are presented below:

(i) By increasing the value of Casson fluid parameters β and magnetic parameter M , the velocity of the flowing fluid is decreasing but the rate of the heat transfer and rate of concentration both are increasing.

(ii) Increasing Prandtl number *Pr,* decreases rate of heat transfer.

(iii) Increasing rate of thermal Radiations *R,* increases the rate of temperature distribution.

(iv) Increasing thermophoresis parameter *Nt* and Lewis number *Le* increase the rate of temperature distribution and rate of concentration.

(v) Combined effect of the Lewis number *Le* and radiation parameter *R* increases the rate of the heat transfer. and reverse to it decreases the rate of concentration or volume fraction.

(vi) Increasing Brownian parameter *Nt,* increases the temperature and reverse to it, decreases the rate of concentration.

(vii) Along the variation of *Nt* or *Nb* at different values of the *Nb* or *Nt* the rate of the heat transfer is increasing but rate of the concentration decrease.

Reference

1. Crane, L. J. Flow past a stretching plate. *Zeitschrift für angewandte Mathematik und Physik ZAMP*, *21*(4), 645-647, (1970).
2. Gupta, P. S., & Gupta, A. S. Heat and mass transfer on a stretching sheet with suction or blowing. *The Canadian Journal of Chemical Engineering*, *55*(6), 744-746, (1977).
3. Grubka, L. J., & Bobba, K. M. Heat transfer characteristics of a continuous, stretching surface with variable temperature. *Journal of Heat Transfer*, *107*(1), 248-250, (1985).
4. Ali, M. E. Heat transfer characteristics of a continuous stretching surface. *Wärme-und Stoffübertragung*, *29*(4), 227-234, (1994).
5. Bakar, N. A. A., Bachok, N., & Arifin, N. M. Nanofluid flow using Buongiorno model over a stretching sheet and thermophysical properties of nanoliquids. *Indian J. Sci. Technol*, *9*, 1-9.5, (2016).

6. Wang, C. Y. Analysis of viscous flow due to a stretching sheet with surface slip and suction. *Nonlinear Analysis: Real World Applications*, *10*(1), 375-380, (2009).
7. Choi, S. U., & Eastman, J. A. *Enhancing thermal conductivity of fluids with nanoparticles* (No. ANL/MSD/CP-84938; CONF-951135-29). Argonne National Lab., IL (United States), (1995).
8. Lee, S., Choi, S. S., Li, S. A., & Eastman, J. A. Measuring thermal conductivity of fluids containing oxide nanoparticles. *Journal of Heat transfer*, *121*(2), 280-289, (1999).
9. Eastman, J. A., Choi, S. U. S., Li, S., Yu, W., & Thompson, L. J. Anomalously increased effective thermal conductivities of ethylene glycol-based nanofluids containing copper nanoparticles. *Applied physics letters*, *78*(6), 718-720, (2001).
10. Aybar, H. Ş., Sharifpur, M., Azizian, M. R., Mehrabi, M., & Meyer, J. P. A review of thermal conductivity models for nanofluids. *Heat Transfer Engineering*, *36*(13), 1085-1110, (2015).
11. Aybar, H. Ş., Sharifpur, M., Azizian, M. R., Mehrabi, M., & Meyer, J. P. A review of thermal conductivity models for nanofluids. *Heat Transfer Engineering*, *36*(13), 1085-1110, (2015).
12. Wang, X., Xu, X., & S. Choi, S. U. Thermal conductivity of nanoparticle-fluid mixture. *Journal of thermophysics and heat transfer*, *13*(4), 474-480, (1999).
13. Liaquat Ali Lund, Zurni Omar, Ilyas Khan, Jawad Raza, Mohsen Bakouri and I. Tlili. Stability Analysis of Darcy-Forchheimer Flow of Casson Type Nanofluid Over an Exponential Sheet: Investigation of Critical Points. Symmetry, (2019). DOI: https://doi.org/10.3390/sym11030412,
14. Lin, Y., Li, B., Zheng, L., & Chen, G. Particle shape and radiation effects on Marangoni boundary layer flow and heat transfer of copper-water nanofluid driven by an exponential temperature. *Powder Technology*, *301*, 379-386, (2016).
15. Buongiorno, J. Convective transport in nanofluids. *Journal of heat transfer*, *128*(3), 240-250, (2006).
16. Khan, W. A., & Pop, I. Boundary-layer flow of a nanofluid past a stretching sheet. *International journal of heat and mass transfer*, *53*(11-12), 2477-2483, (2010).
17. Nield, D. A., & Kuznetsov, A. V. The Cheng–Minkowycz problem for the double-diffusive natural convective boundary layer flow in a porous medium saturated by a nanofluid. *International Journal of Heat and Mass Transfer*, *54*(1-3), 374-378, (2011).
18. Rana, P., Bhargava, R., & Bég, O. A. Numerical solution for mixed convection boundary layer flow of a nanofluid along an inclined plate embedded in a porous medium. *Computers & Mathematics with Applications*, *64*(9), 2816-2832.
19. Makinde, O. D., & Aziz, A. (2011). Boundary layer flow of a nanofluid past a stretching sheet with a convective boundary condition. *International Journal of Thermal Sciences*, *50*(7), 1326-1332.

20. Afify, A. A., & Bazid, M. A. A. (2014). Flow and heat transfer analysis of nanofluids over a moving surface with temperature-dependent viscosity and viscous dissipation. *Journal of Computational and Theoretical Nanoscience*, *11*(12), 2440-2448.

21. Makinde, O. D., Mabood, F., Khan, W. A., & Tshehla, M. S. (2016). MHD flow of a variable viscosity nanofluid over a radially stretching convective surface with radiative heat. *Journal of Molecular Liquids*, *219*, 624-630.

22. Mustafaa, M., Hayat, T., & Obaidat, S. (2013). Boundary layer flow of a nanofluid over an exponentially stretching sheet with convective boundary conditions. *International Journal of Numerical Methods for Heat & Fluid Flow*, *23*(6), 945-959.

23. Rao, M. A. (2010). *Rheology of fluid and semisolid foods: principles and applications*. Springer Science & Business Media.

24. Lund, L. A., Omar, Z., & Khan, I. (2019). Analysis of dual solution for MHD flow of Williamson fluid with slippage. *Heliyon*, *5*(3), e01345.

25. Alarifi, I. M., Abokhalil, A. G., Osman, M., Lund, L. A., Ayed, M. B., Belmabrouk, H., & Tlili, I. (2019). MHD Flow and Heat Transfer over Vertical Stretching Sheet with Heat Sink or Source Effect. *Symmetry*, *11*(3), 297.

26. Mustafa, M., Hayat, T., Pop, I., & Aziz, A. (2011). Unsteady boundary layer flow of a Casson fluid due to an impulsively started moving flat plate. *Heat Transfer—Asian Research*, *40*(6), 563-576.

27. Nadeem, S., Mehmood, R., & Akbar, N. S. (2014). Optimized analytical solution for oblique flow of a Casson-nano fluid with convective boundary conditions. *International Journal of Thermal Sciences*, *78*, 90-100.

28. Mukhopadhyay, S., & Vajravelu, K. (2013). Diffusion of chemically reactive species in Casson fluid flow over an unsteady permeable stretching surface. *Journal of Hydrodynamics, Ser. B*, *25*(4), 591-598.

29. Ferdows, M., Khan, M. S., Alam, M. M., & Afify, A. A. (2017). MHD boundary layer flow and heat transfer characteristics of a nanofluid over a stretching sheet. *Acta universitatis sapientiae, Mathematica*, *9*(1), 140-161.

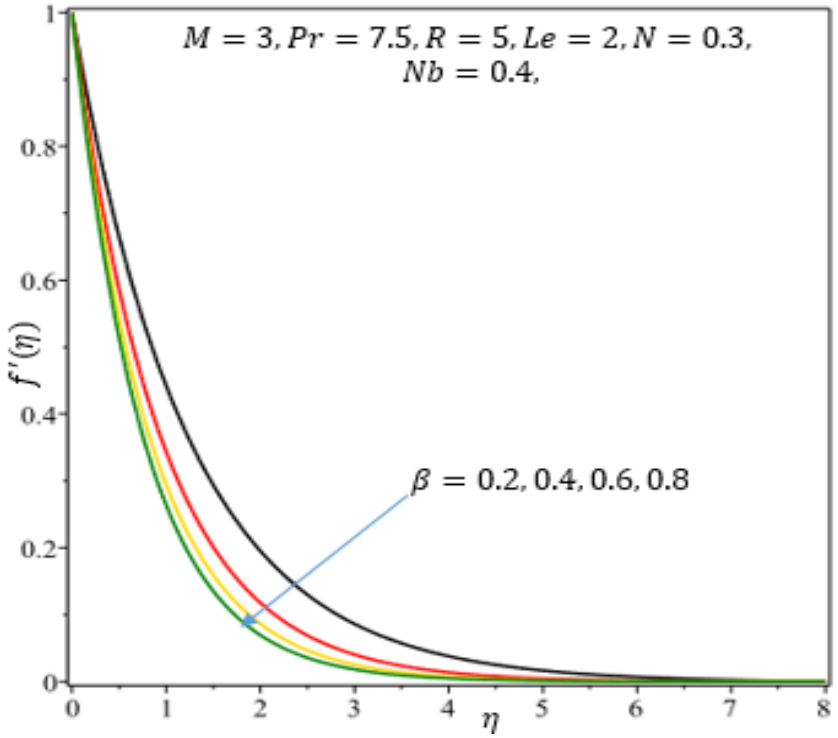

Fig:2. The velocity profile at different values of the of β.

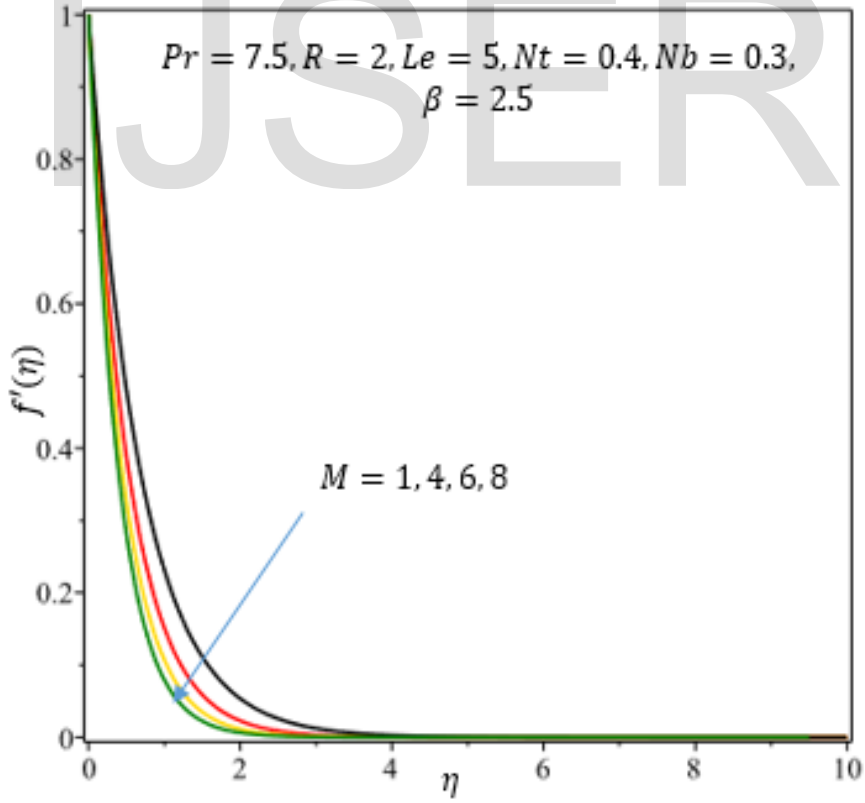

Fig: 3. The velocity profile at different values of the of Magnetic parameter *M*.

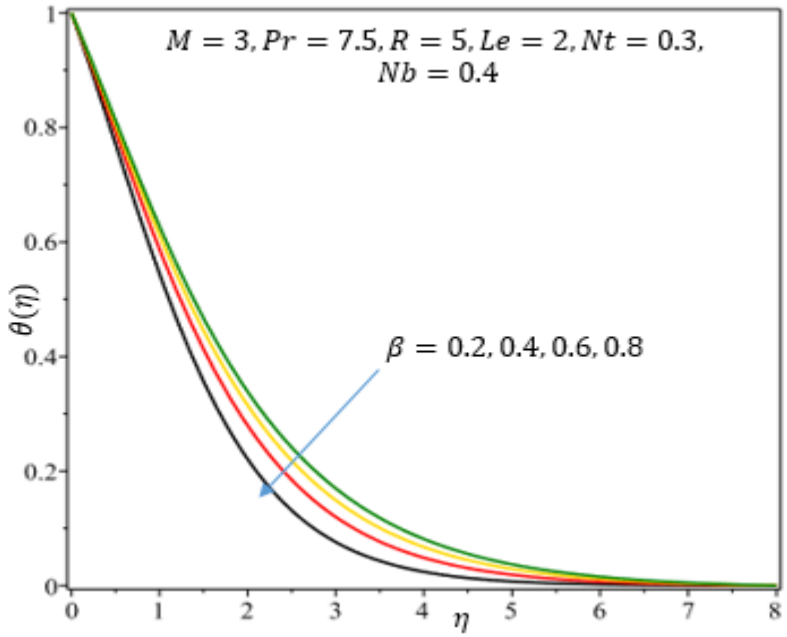

Fig: 4. The temperature profile at different values of the of β.

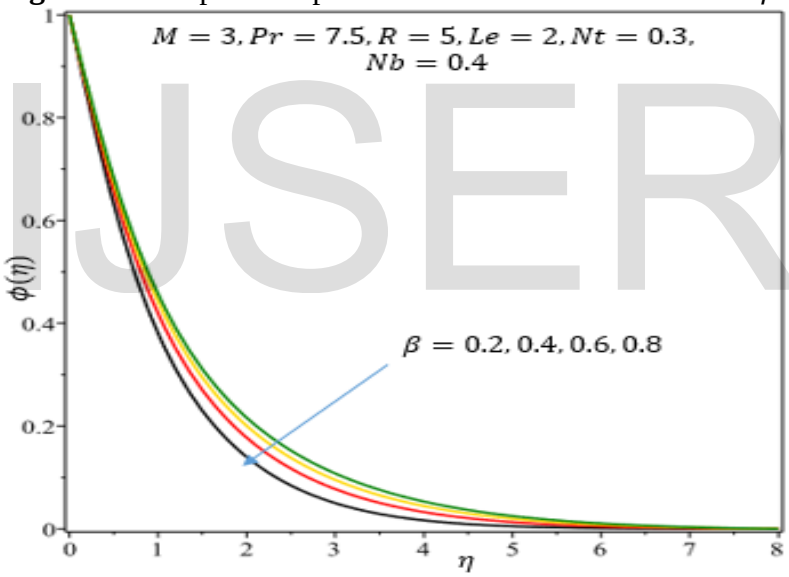

Fig: 5. The nanoparticles concentration profile at different values of the of β.

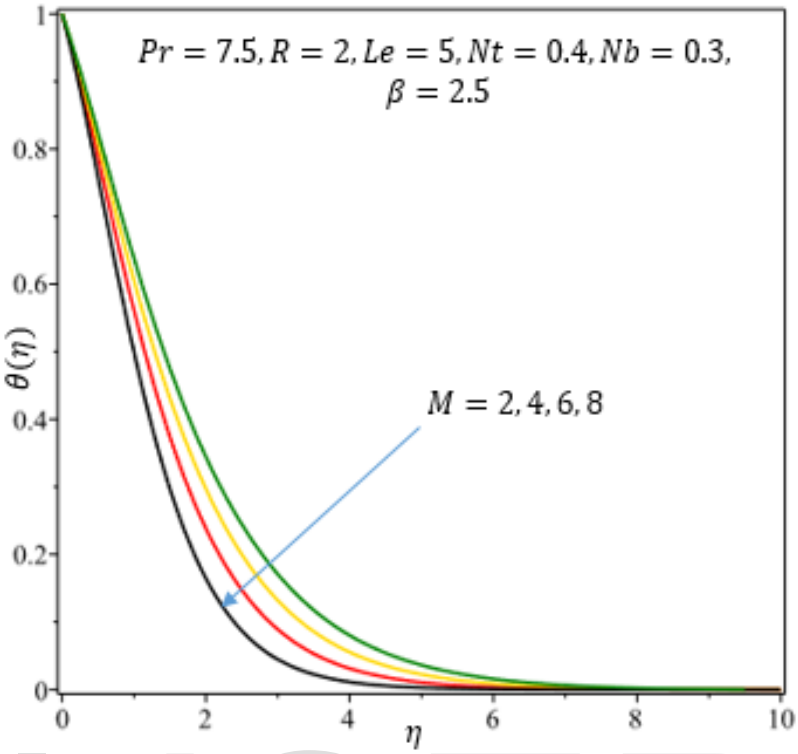

Fig: 6. The temperature profile at different values of the of Magnetic parameter *M*.

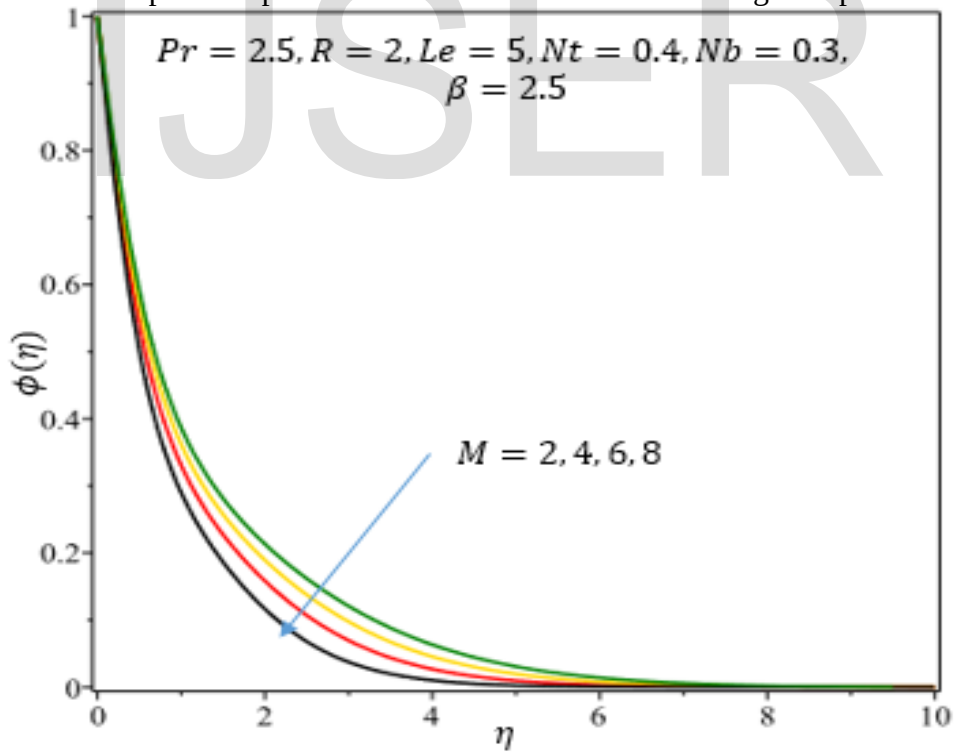

Fig: 7. The nanoparticles concentration profile at different values of the of Magnetic parameter *M*.

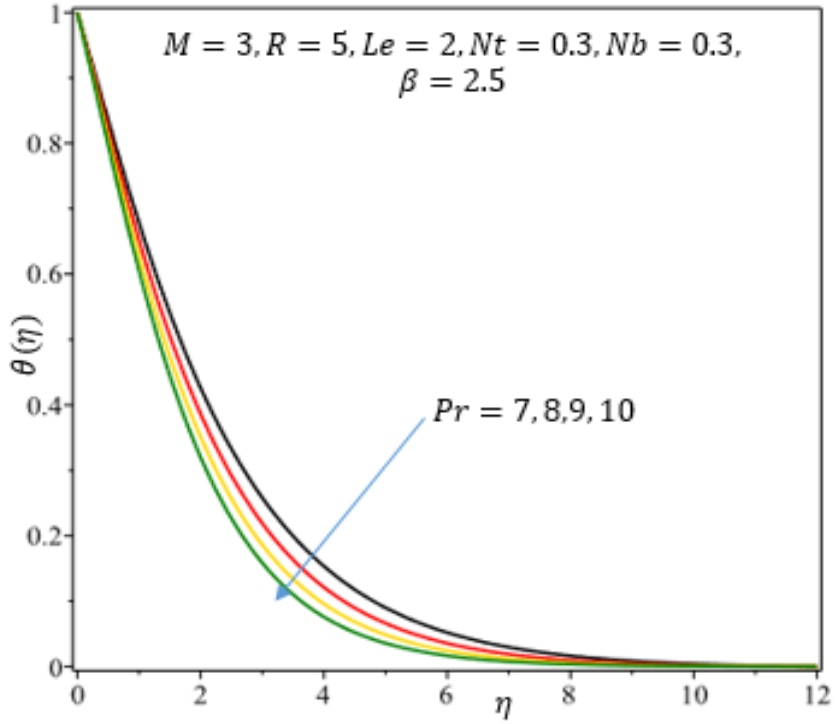

Fig:8. The temperature profile at different values of the of Prandtl number *Pr*.

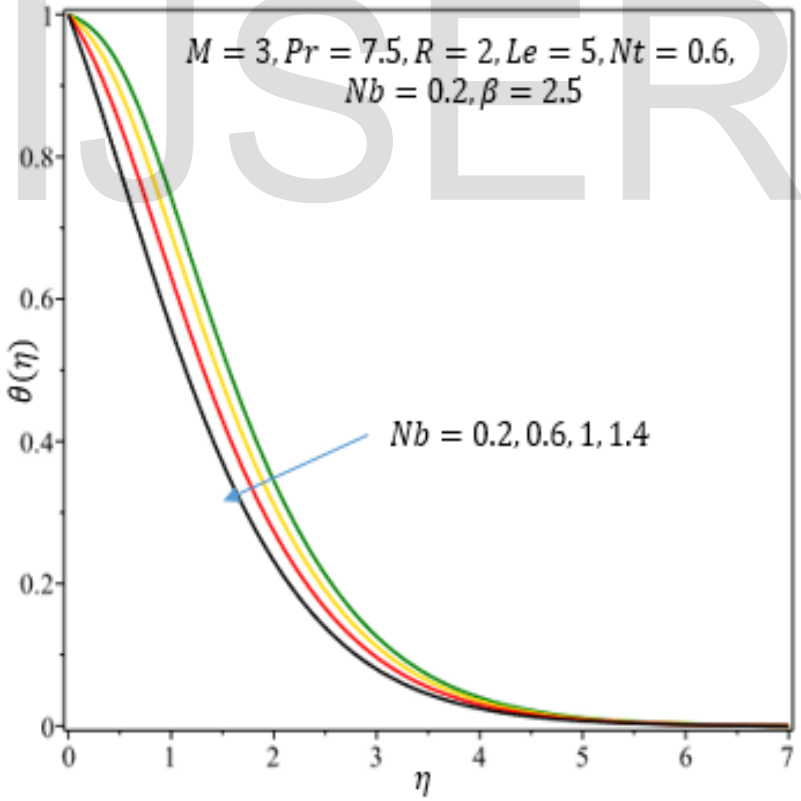

Fig: 9. The temperature profile at different values of the of Brownian motion parameter *Nb*.

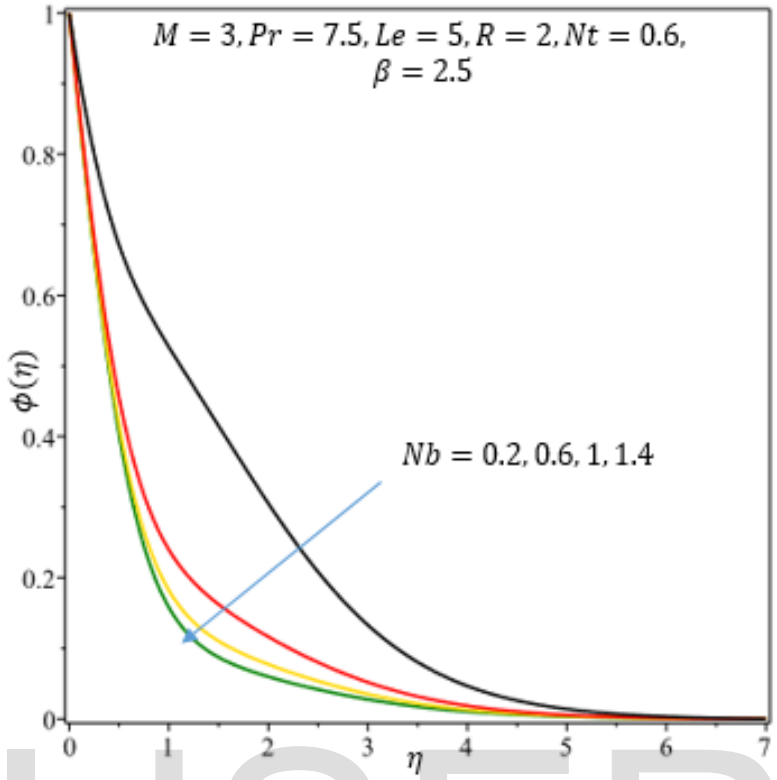

Fig: 10. The nanoparticles concentration profile at different values of the of Brownian motion parameter *Nb.*

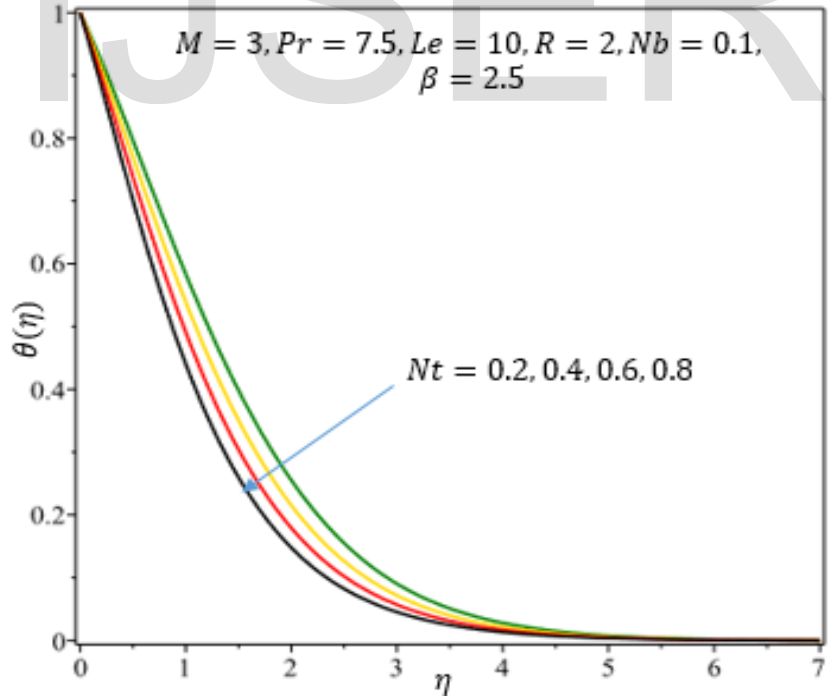

Fig:11. The temperature profile at different values of the of Thermophoresis parameter *Nt.*

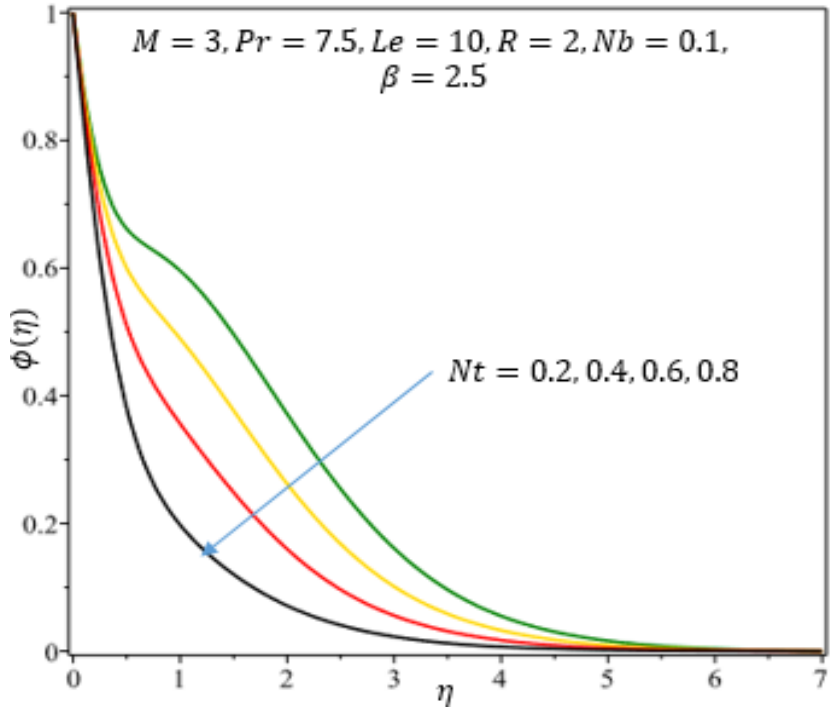

Fig:12. The nanoparticles concentration profile at different values of the of Thermophoresis parameter *Nt.*

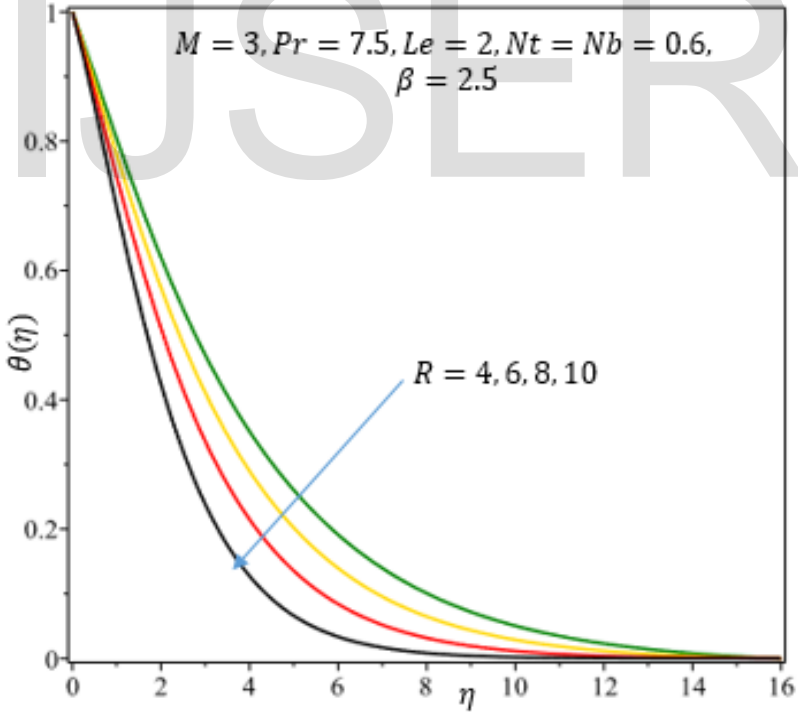

Fig: 13. The temperature profile at different values of of Radiation parameter *R.*

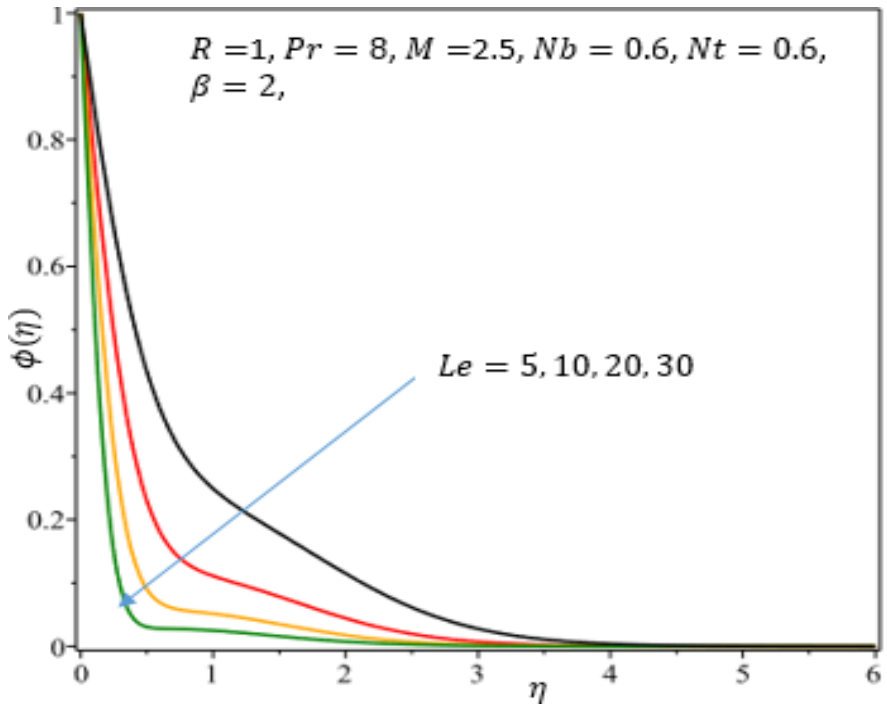

Fig:14. The nanoparticles concentration profile at different values of of Lewis number *Le*.

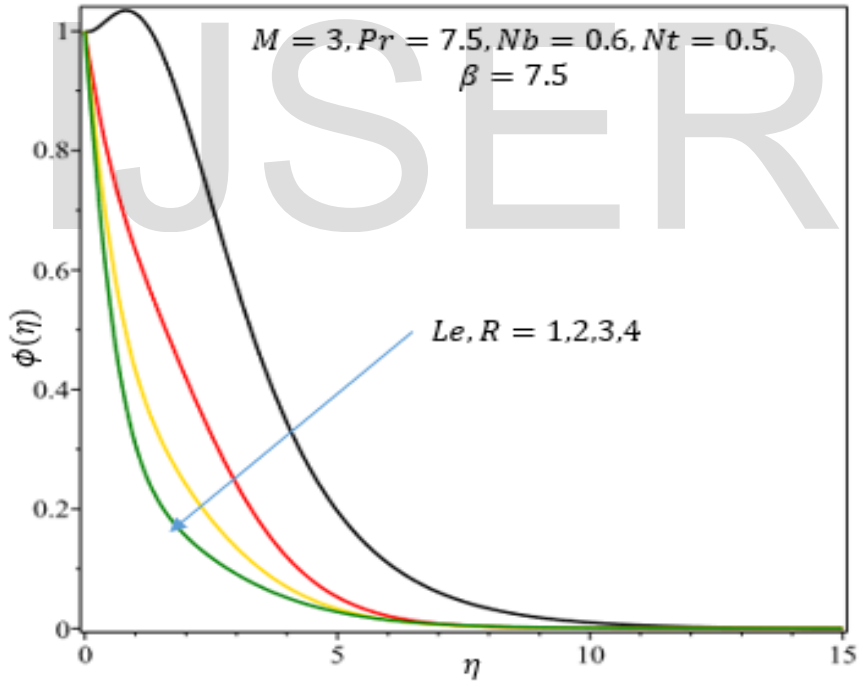

Fig:15. The nanoparticles concentration profile at the different values of of *Le* and *R*.

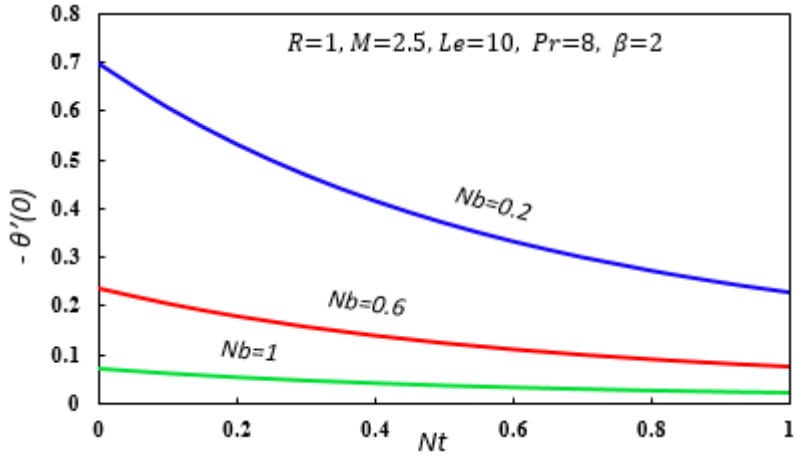

Fig:16 The effect of *Nb* along variation of the *Nt* on non-dimensional heat transfer rate.

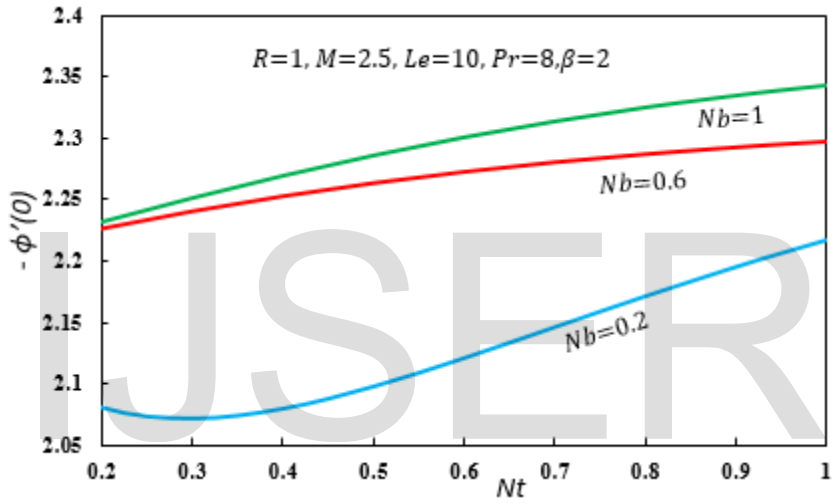

Fig: 17. The effect of *Nb* along variation of the *Nt* on non-dimensional heat transfer rate

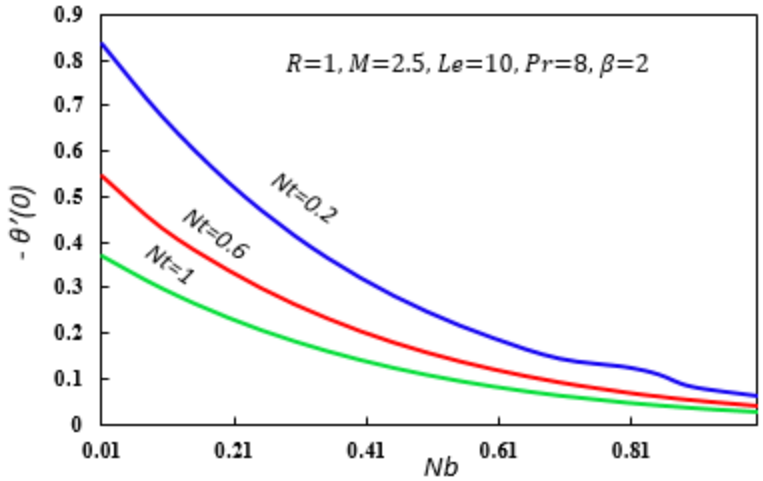

Fig: 18. The effect of *Nt* along variation of the *Nb* on the non-dimensional heat transfer rate.

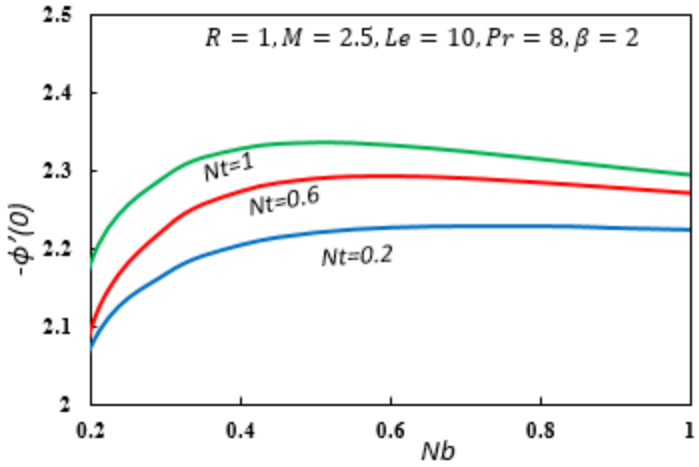

Fig: 19. The effect of *Nt* along variation of the *Nb* on mass transfer coefficient.